Experimental Investigation of Water Wave Characteristics in a Wave Channel

Mohammed Faizal [1], M. Rafiuddin Ahmed[1*]
[1]Division of Mechanical Engineering, The University of the South Pacific
Laucala Campus, Suva, Fiji

Chang-Goo Kim[2] and Young-Ho Lee[2]
[2]Division of Mechanical and Information Engineering, Korea Maritime University
1 Dongsam-Dong, Youngdo-ku, Busan 606-791, Korea

[*]Corresponding author. Email : ahmed_r@usp.ac.fj

Abstract

A deeper understanding of the water wave characteristics is essential for designing efficient energy extraction devices. An experimental study of the characteristics of waves was performed in a two-dimensional wave channel by varying the mean depth of water and the wave frequency. The orbital motion of particles in water waves has been of interest to researchers from both academic and practical perspectives. This orbital motion, which results from the directional velocities of the particles under waves at different phase positions, was studied with particle image velocimetry (PIV) measurements and compared with theoretical calculations. The kinetic energy and the size of the orbits were found to be larger near the surface and reduce with increasing depth. It was also found that the wavelength reduces with increasing frequency as well as for reducing mean water depths, while the wave height and the wave power increase with frequency (for non-breaking waves). The wave power was found to be the highest for the case of maximum mean water depth in the wave channel.

Key words : Wave characteristics, wave energy, orbital motion, experimental fluid mechanics, particle image velocimetry

Introduction

Water waves propagate on the ocean surface as a result of a generating force [1]. The most common generating force for water waves is the moving air or wind. Energy is transferred from the wind to the water by the frictional drag of the air on the ocean surface, thus creating waves [2]. Water waves are always present on the ocean surface as long as there is wind blowing over the ocean, thus offering an infinite source of wave energy. Water waves can be classified into two categories: oscillatory waves and translatory waves. In oscillatory waves, the average mass transport of water is zero. Translatory waves involve the mass transport of water in the direction of wave travel [3]. Examples of translatory waves are waves formed by floods in rivers and tidal bores. The simplest way to study waves is by assuming them to be regular sinusoids [4,5]. Common characteristics of a sinusoidal wave are the wave period (T), the wavelength (L) and the wave height (H). Water wave motions are complex and irregular on the ocean surface. Mathematical analysis becomes easier when idealized solutions are considered. Experimentally, it is convenient to study two-dimensional waves in channels with parallel side-walls. Boundary layer effects can be neglected as they are very small [3].

1. Background

A study of the ocean waves and their characteristics is essential for the design of ocean structures and of energy extraction devices. Intrusive techniques of flow field measurements such as velocity probes disturb the flow of the particles. Modern instrumentation allow accurate measurements of wave parameters [6,7]. Particle image velocimetry (PIV) is now a standard optical method for instantaneous mapping of flow fields and can measure particle velocities over a large 2-D area of a flow field. The flow is seeded with particles, which are illuminated and their positions recorded photographically [8,9].

Considering oscillatory waves, it is only the wave-form that moves through the water, and not the water particles [4,5]. The motion of the waves sets the water particles in orbital motion [10,11]. A water wave is a combination of both longitudinal and transverse wave motions. In longitudinal motion, the particles oscillate back and forth parallel to the direction of wave propagation, instead of moving with the wave. In transverse motion, the particle displacement is perpendicular to the

direction of the wave transmission. The particles do not move with the wave, but oscillate up and down about their individual stable positions [12]. The two separate motions of the particles combine to give the overall orbital motion. As the waves are formed, the surface water particles rise and move forward with the crest. When the crest passes, the particles slow down and fall during the forward motion. When the trough advances, particles slow their falling rate and move backward. When the trough passes, the particles slow their backward speed and start to rise and move forward with the crest [11]. These movements of water particles result from the longitudinal and transverse oscillations and create the orbital path.

Orbital motion of particles is present in both deep water waves (mean water depth, $D > L/2$) and in shallow water waves ($D < L/20$). However, the orbit is circular in deep water waves, whereas it is elliptical in shallow water waves with the major axis in the horizontal direction. The motions of the particles are shown in Fig. 1. For deep water waves, the particle displacements, velocities, and oscillations decrease exponentially with increasing depth below the mean level. The effect of the wave motion is reduced to about 0.043 of its surface amplitude at a depth of $L/2$ below the surface [13]. In shallow water, the length of the minor axis of the elliptical orbits decreases with increasing depth while that of the major axis remains constant till the bottom; which means the effect of waves is felt till the bottom [10]. Waves that fall in between shallow and deep water, $L/20 < D < L/2$, are termed as intermediate depth waves. Mathematical analysis is mostly done for shallow and deep water waves, since the governing equations do not simplify for intermediate depth waves [14].

Water waves have energy associated with them: kinetic energy of the moving particles and potential energy due to the vertical position of the water from the mean level. The total energy is proportional to the square of the wave height and is equally divided between kinetic and potential energies [15,16]. A higher wave will have more potential and kinetic energies. A number of devices are now developed to extract energy from the waves [15,17-19]. Wave energy is attracting a lot of attention now, as it is available 90% of the time at a given site compared to solar and wind energies which are available 20-30% of the time [18]. According to McCormick [19], there are some basic concepts on which wave energy extraction devices are based. Heaving and pitching bodies make use of the surface

displacement of water as an energy source. Pressure devices utilize the hydrostatic and dynamic pressure changes beneath the water waves. Surging wave energy converters capture wave energy as waves enter the surf zone. Cavity resonators make use of the displacement of water in a water column. Particle motion converters obtain energy from the moving water particles. The moving elements of the energy extraction device should have their motions matching those of the orbiting water particles [20].

The present work is aimed at studying the characteristics of the waves in a wave channel. A deeper understanding of the water wave characteristics is essential from both academic and practical perspectives. There are very few reported works on such studies, which provided the motivation for this work.

2. Experimental Setup and Procedure

The experiments were carried out in a *Cussons* Wave Channel, model P6325, available in the Thermo-fluids laboratory of the University of the South Pacific. The wave channel has a length of 3500 mm, a width of 300 mm and a depth of 450 mm. The side walls are made of Plexiglas to allow a clear view of the wave action. A flap type wave-maker, hinged at the bottom, produces oscillatory, sinusoidal waves with characteristics of deep water waves [21]. A frequency range of 0 to 1.4 Hz can be set. The close fit of the wave-maker to the channel sides ensures that 2-D waves are produced with no fluid motion normal to the sidewalls [7,21]. Figure 2 shows a schematic diagram of the wave channel. The water flow is generated by a centrifugal pump having a rated capacity of 40 Lit/s at a total head of 10 m and driven by a 5.5 kW motor.

The pump draws water from a tank of 1.5 m x 0.8 m cross-section which receives back the same water from the wave channel. To minimize reflection of the waves, a Cussons Tuneable Beach, model P6285, was installed at the end of the wave channel. It employs a series of porous plates with different porosity levels to absorb the wave energy gradually. The use of different plates with a variable spacing between them allowed a wide variety of wave profiles to be absorbed.

The wave height and the wavelength were measured using Seiki pressure transducers, model PSHF002KAAG. The data were acquired on a GL500A midi-LOGGER dual data logger, which was

connected to the pressure transducers. The wave period was measured by recording the time taken for two successive crests to pass a given point. The wave frequency is calculated by taking the reciprocal of the wave period and was varied from 0.58 Hz to 1.1 Hz. The wave parameters were varied by changing the frequency of the wave maker. The water depth (still water level from the bottom of the tank) was varied from 240 mm to 300 mm during the experiments.

PIV measurements were performed to study the orbital motion of water particles at various frequencies and mean water depths. Poly Vinyl Chloride tracer particles, with an average diameter of 100 μm and a specific gravity of 1.02, were seeded in the water. A 500mW air-cooled Diode-Pumped Solid State continuous light laser with an output of 532 nm was employed to obtain a laser sheet and illuminate the particles. The motion of the particles was captured by a high-speed *Photron* CCD camera. The camera recorded 125 frames per second, producing up to 1280 x 1024 pixel images. The images captured by the CCD camera were processed using *Cactus 3.3* software. Figure 3 shows the PIV set-up and the wave channel. The factors which were considered for determining the accuracy of velocity measurements with PIV are: the uncertainties due to finite time sampling, finite displacement of the particles, and uncertainties in measuring the displacements of the particle images [9]. The accuracy of displacement measurements with *Cactus* is of the order of 0.1 pixel. For the high speed camera, the time resolution for the current measurements was 0.008 s. To get an accurate estimate of the uncertainty in our measurements, most of which were for rotating (orbital) motion of particles, PIV measurements were performed on a calibrated, constant speed rotating motion and the maximum error was found to be 0.32%.

3. Results and Discussion

The results are presented and discussed in this section. Figure 4 shows the variation of the wavelength with frequency for different depths. A theoretical comparison was done with the linear wave theory presented by Dean and Dalrymple [1], as well as the theory presented by Roux [22,23] for waves in different water depths for a horizontal bottom. The wave period and the water depth from the experiments were the starting parameters in the theoretical analyses. It can be seen that for a given wave frequency, the wavelength increases as the mean water depth is increased. It is interesting to

note that the wavelengths are larger for greater mean water depths. The trends for wavelengths are similar but the theoretical values vary with experimental results by more than 50%, with the Roux theory predicting the maximum values. The peculiarity of the wave channel, in which the energy is imparted to the water only at one end, as compared to the continuous transfer of energy from air to water in ocean waves is one of the reasons for the difference in experimental and theoretical values.

The variation of the wave height with frequency at different depths can be seen in Fig. 5. From experimental results, it is clear that the wave height increases with frequency. The wave heights are higher for greater depths and the maximum wave heights are recorded for the maximum mean water depth of 300 mm, indicating that the energy transfer from the wave-maker to the water is maximum for the case of maximum depth due to the maximum area of contact between the wave maker flap and water. Not surprisingly, these results are not in agreement with the theory of Roux [22,23] for waves in different water depths for a horizontal bottom. The wave heights decrease with increasing frequency and the maximum wave height is recorded for the minimum depth of 240 mm. Roux [22,23] presented his theory for fully developed sea conditions whereas we are presenting experimental wave characteristics for waves generated in a wave channel. Because of the increased contact area between the flap of the wave-maker and the water for greater mean water depths, higher energy is transferred to the water which results in higher wave heights.

Detailed PIV measurements were performed to study the motion of the water particles to gain a better understanding of the orbital motion at different wave frequencies and mean water depths. The velocity vectors at a frequency of 0.7 Hz and mean water depth of 260 mm for the cases when the crest and the trough are at the middle of the measurement grid, phase positions $\theta = 0^o$ and 180^o, are shown in Figs. 6 and 7 respectively. The velocities at the instance when the crest is in the measurement grid are oriented in the down-wave direction and when the trough is in the measurement area, they are oriented in the up-wave direction. It can also be seen that the vectors are pointing right-downwards before the crest ($\theta = 270^o$ to 360^o) and right-upwards after the crest ($\theta = 0^o$ to 90^o).

Similarly, the vectors are pointing left-upwards before the trough ($\theta = 90^o$ to 180^o) and left-downwards after the trough ($\theta = 180^o$ to 270^o). At the phase position $\theta = 90^o$, the movement of

particles is upwards (no component in the horizontal direction) and at the phase position $\theta = 270^o$, the movement of particles is downwards (no component in the horizontal direction). This is also supported by theoretical analysis [1,16]. The Ursell number (HL^2/D^3) in the present studies was less than 10 indicating that the waves generated are not really linear [3]. The variations of the horizontal and vertical components of particle velocities (u and w respectively) with depth were studied in detail and a comparison with the theoretical variation was made. The two components of velocity are given by

$$u = \frac{gHT}{2L}\frac{\cosh[k(z+D)]}{\cosh kD}\cos\theta + \frac{3}{8}\frac{\pi gH^2T}{L^2}\frac{\cosh[2k(z+D]}{\sinh^3 kD\cosh kD}\cos 2\theta$$

$$w = \frac{gHT}{2L}\frac{\sinh[k(z+D)]}{\cosh kD}\sin\theta + \frac{3}{8}\frac{\pi gH^2T}{L^2}\frac{\sinh[2k(z+D)]}{\sinh^3 kD\cosh kD}\sin 2\theta$$

where k is the wave number given by $k = 2\pi/L$.

The horizontal velocities in the positive x-direction were found to be the maximum under the crest for all the cases studied (e.g. Fig. 6) with the magnitude reducing with depth. On the other hand, the horizontal velocities in the negative x-direction were found to be the maximum under the trough (e.g. Fig. 7). The magnitudes of the mean velocities under the crest and the trough reduced by nearly 60% from the highest measurement point to a depth of 200 mm. Liu et al. [24] from their LDA and PIV measurements reported a reduction of about 75% in the magnitude of the mean velocities under the crest and the trough. The magnitudes of the velocities are smaller at lower frequencies and increase at higher frequencies.

Based on the wave parameters at D = 260 mm and using the equations for u and v above, a theoretical analysis was done for the particle velocities at a submergence of 70 mm below the mean level, for a frequency of 0.7 Hz. The resultant velocities of a particle at different phase positions are shown in Fig. 8. It can be seen that at $\theta = 0^o$, the velocity is in positive x-direction, at $\theta = 90^o$, the velocity is vertically upwards, at $\theta = 180^o$, the velocity is in the negative x-direction, and at $\theta = 270^o$, the particle velocity is directed vertically downwards. On either side of $\theta = 90^o$, the velocities are directed towards each other whereas the velocities are directed in the opposite directions at $\theta = 270^o$. These directional

velocities are in good agreement with PIV results. The maximum velocity calculated is 0.259 m/s, which is also comparable with PIV results (Figs. 6 and 7).

The velocity vectors at a frequency of 1.1 Hz for the case of $\theta = 270^o$ at the middle of the measurement grid are shown in Fig. 9. A considerably high kinetic energy of the particles was recorded at this high frequency compared to lower frequencies. It is interesting to observe that the velocity vectors at this phase position are directed downwards and the horizontal component of velocity is almost zero, perfectly matching the theoretical results. The upward-moving particles at $\theta = 90^o$ (not shown) and the downward-moving particles at $\theta = 270^o$ contribute to a full orbit in combination with the down-wave motion of particles under the crest (eg Fig. 6) and the up-wave motion of particles under the trough (e.g. Fig. 7). It was also observed that the particles crowd together near the crest (not shown), whereas they separate in the trough (Fig. 9). In other words, the surface 'shrinks' at the crest and 'expands' in the trough [16]. As discussed earlier, the surface water particles rise and move forward with the crest getting bunched together. With the advancement of trough, the particles slow their falling rate and are separated apart.

The experimental wave height increases with frequency, as shown in Fig. 5. A higher wave has larger orbits of particle motion [15]. From the PIV results, it is clear that the orbital size is increasing with frequency. There is a transfer of energy or momentum from this orbital motion of the water particles just above the turbulent boundary layer to the turbulent motion in the layer. This transfer depends on the wave field and the characteristics at the bottom [15]. Also, the wave action reduces significantly with increasing depth. As a result of these, the velocity vectors tend to become nearly horizontal near the bottom (bed) of the wave channel.

The distribution of the kinetic energy at a frequency of 1.1 Hz and the depth of 260 mm can be seen in Fig. 10. This corresponds to the instant when the wave crest has just entered the measurement grid. The kinetic energy at this frequency is significantly higher compared to the lower frequencies. It should be noted that, not only the kinetic energy, but also the potential energy will be higher close to the free surface of water because of the height from the mean level. The kinetic energy decreases with increasing depth below the mean water level.

The variation of the wave power per unit width with wave frequency at different mean water depths is shown in Fig. 11. The wave power per unit width of the crest (P) is calculated from the wave height and the wave period using the relation

$$P = \frac{\rho g^2 H^2 T}{32\pi}$$

It can be seen that the wave power increases continuously with increasing frequency at all mean water depths. This is due to the increase in the wave height with frequency and the higher wave heights at greater depths (Fig. 5). However, due to wave breaking (ratio of wave height to wavelength is 1:7), the power available will reduce because the wave height decreases. Wave breaking is not encountered in the present studies.

Conclusions

The characteristics of water waves were studied experimentally in a wave channel at different mean water depths and wave frequencies. It was found that the wavelength reduces with increasing wave frequency. Higher values of wavelength were recorded for greater mean water depths. The wave height increased with wave frequency and higher wave heights were recorded for greater mean water depths due to higher transfer of energy from the wave-maker to the water. The movement of water particles was studied in detail and the orbital motion of particles was captured with PIV measurements. The directional velocities of the particles under waves at different phase positions combine to give the overall orbital motion of the particles. It was found that the orbital size increases with wave frequency. The maximum kinetic energy and the size of the orbits are closer to the surface. The wave power was found to increase with wave frequency (for non breaking waves) and the highest wave power per unit width of the wave crest was recorded at the maximum mean water depth in the wave channel.

Acknowledgements

The authors acknowledge the help rendered by Young-Jin Cho and Krishnil Prasad during setting up of the experiments and data acquisition.

REFERENCES

1. Dean, R.G. and Dalrymple, R.A., *Water Wave Mechanics for Engineers and Scientists*, World Scientific Publishing Co., Singapore, 1991.

2. Janssen, P., *The Interaction of Ocean Waves and Wind*, Cambridge Univ Press, United Kingdom, 2004.

3. LeMéhauté, B., *An Introduction to Hydrodynamics and Water Waves*, Springer-Verlag, New York, 1976.

4. Lighthill, J., *Waves in Fluids*, Cambridge Univ Press, New York, 2001.

5. Pickard, G.L. and Pond, S., *Introductory Dynamical Oceanography*, Butterworth-Heinemann, Oxford, 1986.

6. Graw, K.U. and Lengricht, J., Comparison of LDV and Ultrasonic Measurement of Orbital Velocity, *Proc. XXV IAHR Congress*, Tokyo, Japan, 1993, pp. 81-88.

7. Gray, C, and Greated, C.A., The Application of Particle Image Velocimetry to the Study of Water Waves, *Optics and Lasers in Eng*, 1988, **9**, pp. 265-276.

8. Stagonas, D. and Muller, G., Wave Field Mapping with Particle Image Velocimetry, *J. Ocean Eng*, 2007, **34**, pp. 1781-1785.

9. Raffel, M., Willert, C. and Kompenhans, J., *Particle Image Velocimetry – A Practical guide*, Springer, Berlin Heidelberg, 1998.

10. Sverdrup, K.A., Duxbury, A.B. and Duxbury, A.C., *Fundamentals of Oceanography*, McGraw Hill, New York, 2006.

11. Constantin, A., On the Deep Water Wave Motion, *J. Phys. A: Math. Gen.*, 2001, **34**, pp 1405-1417.

12. Russell, D., *Longitudinal and Transverse Wave Motion*, online http://www.gmi.edu/~drussell/Demos/waves/wavemotion.html, 2001.

13. Bowden, K.F., *Physical oceanography of coastal waters*. Ellis Horwood Ltd, Chichester, 1983, p. 80.

14. Rahman, M., *Water waves - Relating Modern Theory to Advanced Engineering Practice*, Oxford Univ. Press, New York, 1994.

15. Falnes, J., A Review of Wave-Energy Extraction, *Marine Structures*, 2007, **20**, pp. 185-201.

16. Holthuijsen, L.H., *Waves in Oceanic and Coastal Waters*, Cambridge Univ Press, United Kingdom, 2007.

17. Twidell, J. and Weir, A.D., *Renewable Energy Resources*, Taylor and Francis, New York, 2006.

18. Pelc, R. and Fujita, R.M. Renewable Energy from the Ocean, *Marine Policy*, 2002, **26**, pp. 471-479.

19. McCormick, M.E., *Ocean Wave Energy Conversion*, Dover Publications, New York, 2007.

20. Faizal M., Ahmed M.R., Lee, Y.H., On utilizing the orbital motion in water waves to drive a Savonius rotor. *Renewable Energy*, 2010, **35**, pp. 164-169.

21. Rea, M. “Wave Tank and Wave-maker Design,” in: João Cruz, *Ocean Wave Energy – Current Status and Future Perspectives*, Springer, Berlin Heidelberg, 2008, pp. 147-159.

22. Roux, J.P.L., An extension of the Airy theory for linear waves into shallow water, *Coastal Engineering*, 2008, **55**, pp. 295-301

23. Roux, J.P.L., Profiles of fully developed (Airy) waves in different water depths. *Coastal Engineering*, 2008, **55**: 701-703.

24. Liu, A. Shen, X., Smith, G.H. and Grant, I., “Particle Image Velocimetry Measurements of Wave-Current Interactions in a Laboratory Flume,” *Optics and Lasers in Eng*, 1992, **16**, pp. 239-264.

List of Figures

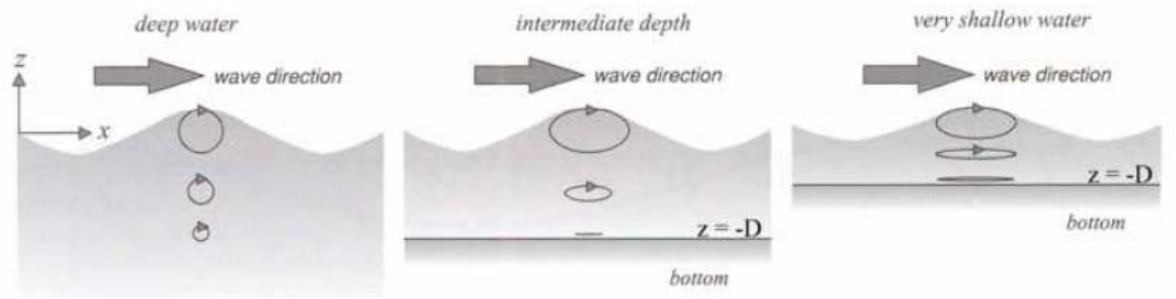

Fig. 1. The orbital motion in deep water, intermediate-depth water and shallow water [16].

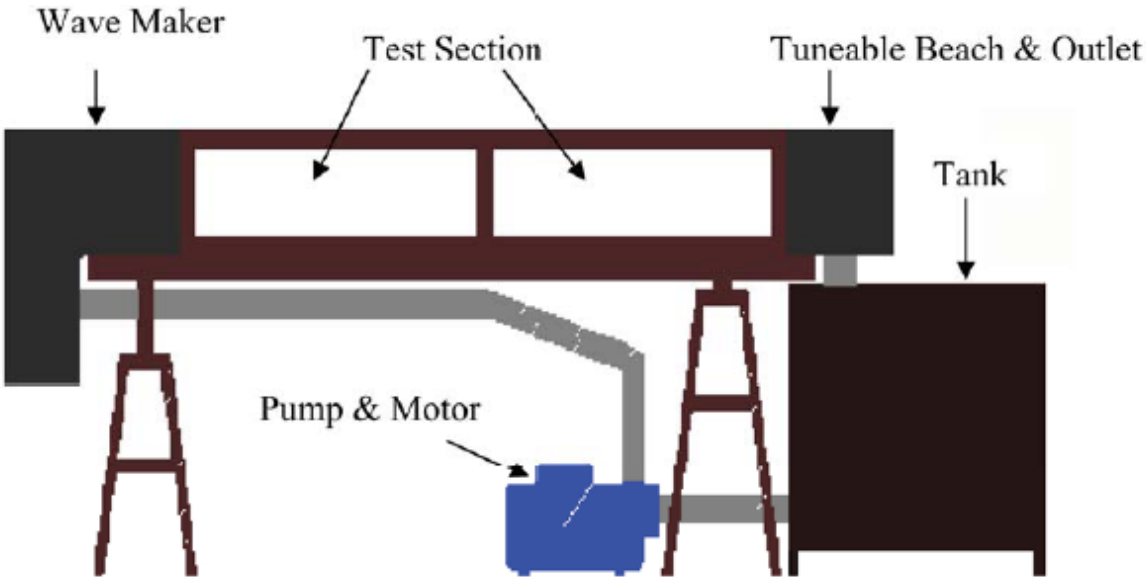

Fig. 2. Schematic diagram of the Wave Channel.

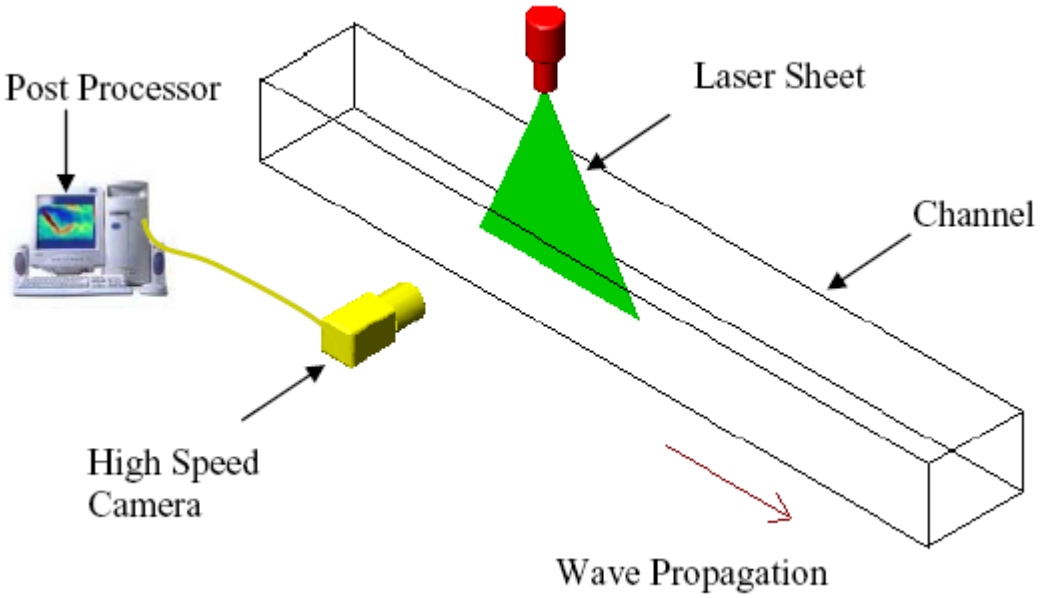

Fig. 3. Schematic of the PIV set-up.

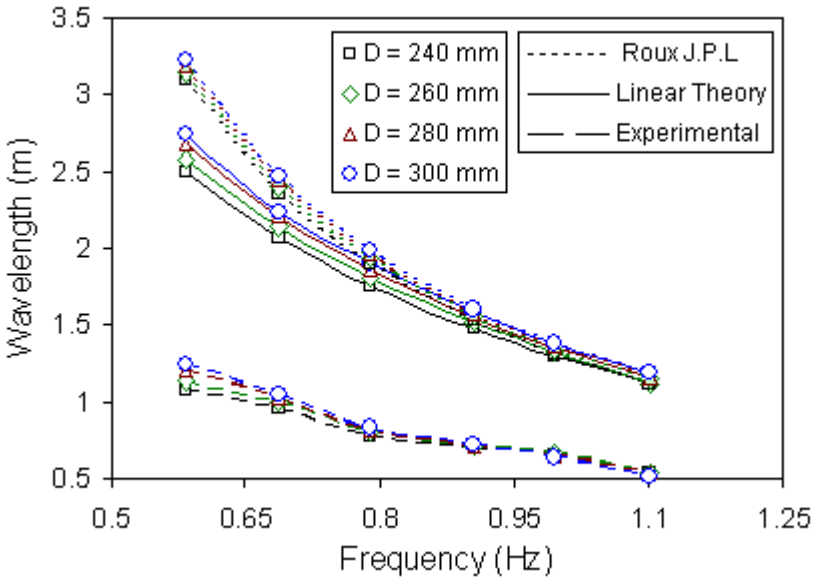

Fig. 4. Variation of the wavelength with frequency at different water depths.

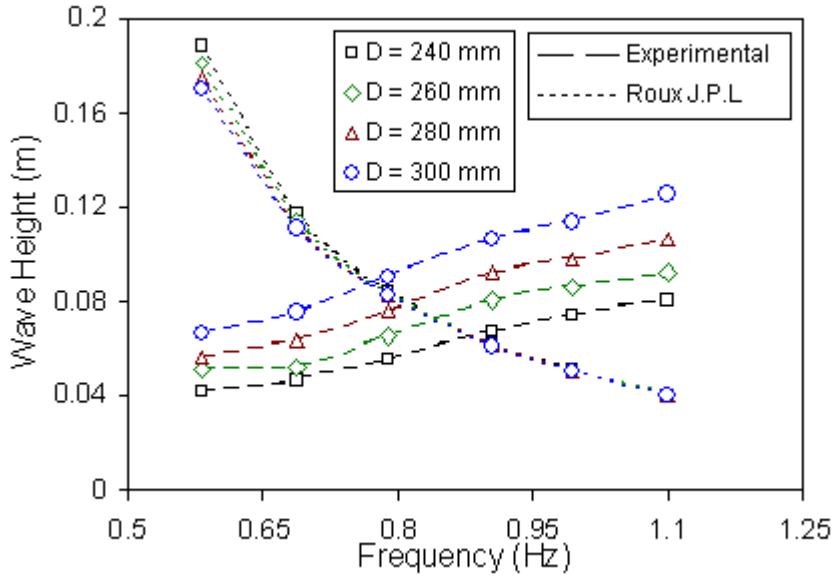

Fig. 5. Variation of the wave height with frequency at all water depths.

Separate image file

Fig. 6. Velocity vectors when the crest is at the middle of the measurement grid for a depth of 260 mm and a frequency of 0.7 Hz.

Separate image file

Fig. 7. Velocity vectors when the trough is at the middle of the measurement grid for a depth of 260 mm and a frequency of 0.7 Hz.

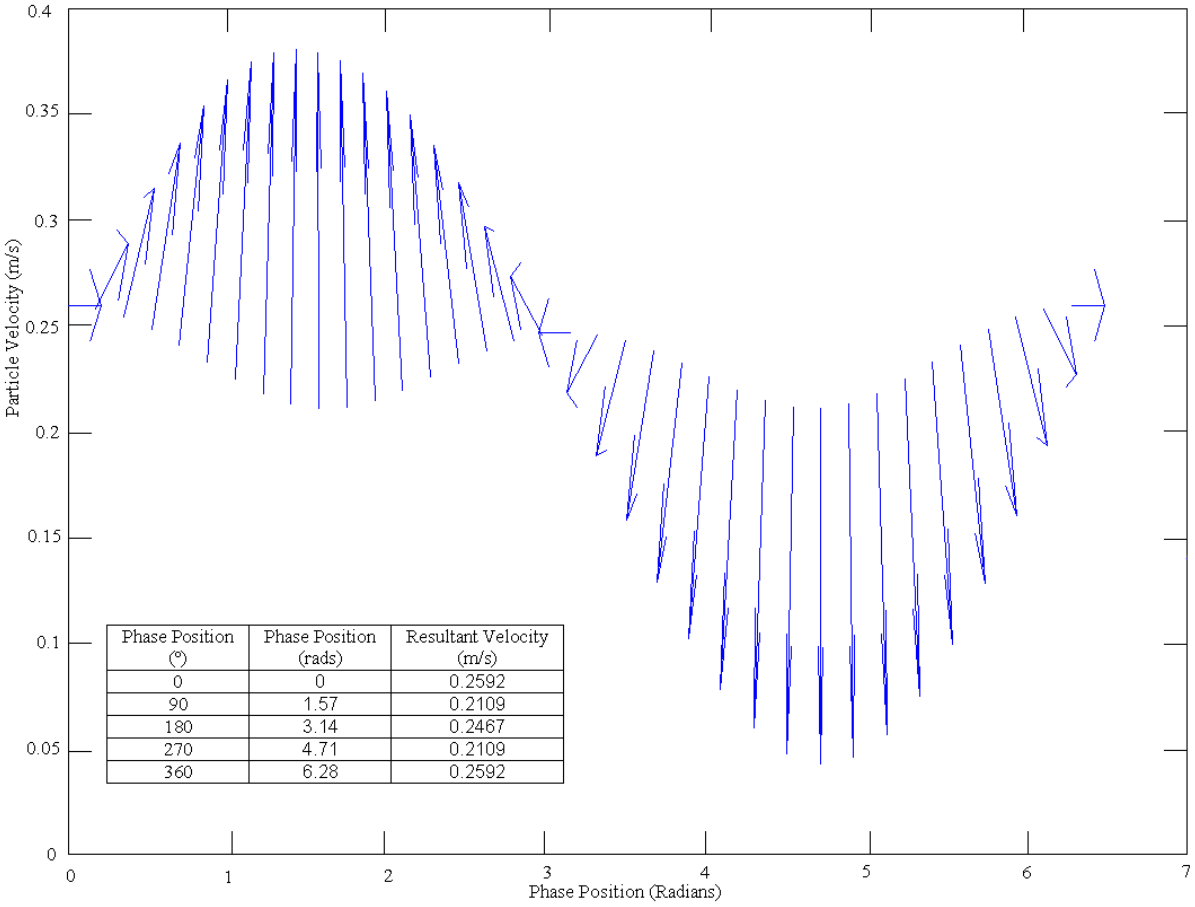

Phase Position (°)	Phase Position (rads)	Resultant Velocity (m/s)
0	0	0.2592
90	1.57	0.2109
180	3.14	0.2467
270	4.71	0.2109
360	6.28	0.2592

Fig. 8. The theoretical resultant velocities of a particle at different phase positions at a submergence of 70 mm below the mean level, for a frequency of 0.7 Hz and a water depth of 260 mm.

Separate image file

Fig. 9. Velocity vectors for the case of $\theta = 270^{o}$ at the middle of the measurement grid for a depth of 260 mm and a frequency of 1.1 Hz.

Separate image file

Fig. 10. Contours of iso-kinetic energy for a depth of 260 mm and a frequency of 1.1 Hz.

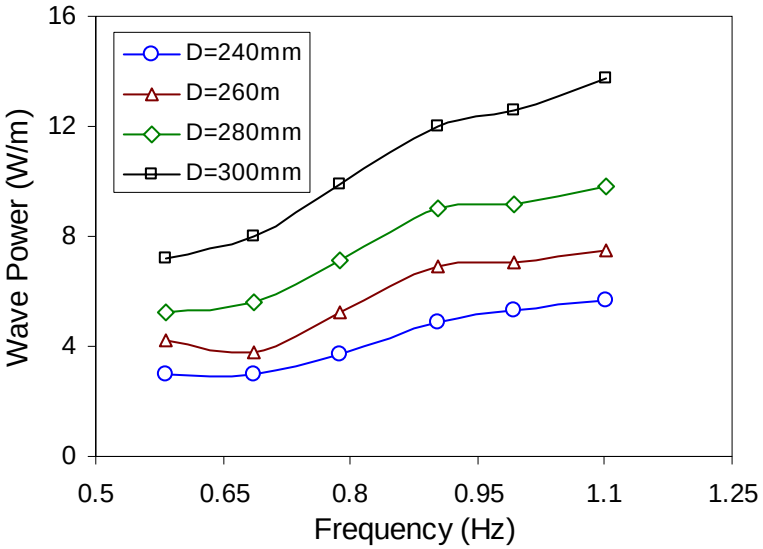

Fig. 11. Variation of wave power with frequency at different water depths.